A New Strategy for Dynamic Weighing in Motion of Railway Vehicles

A New Strategy for Dynamic Weighing in Motion of Railway Vehicles

Benedetto Allotta, *Member, IEEE*, Pierluca D'Adamio, Lorenzo Marini, Enrico Meli, *Member, IEEE*, Luca Pugi, and Andrea Rindi

***Abstract*—Weighing-in-motion (WIM) systems automatically perform the dynamic weighing of railway vehicles while the trains are running on the lines through a reasonable number of measurement points placed along the track. Such intelligent systems may overcome disadvantages in terms of costs and traffic management, which are typical of conventional static weighing systems. In this paper, we present an innovative algorithm for dynamical WIM applications aimed at estimating the axle and wheel loads of a generic train composition by means of indirect track measurements. The new approach allows the axle loads estimation at high vehicle speeds and can be customized for several input track measurements (rail shear, rail bending, vertical forces on the sleepers, etc.) as well as a combination of them. Consequently, it can be employed in different kinds of measurement stations. Having once studied the accuracy of the algorithm in estimating the loads, the same novel procedure is used to estimate the center-of-gravity position of the railway vehicle to avoid dangerous imbalances. The algorithm can receive as inputs both experimental and simulated data; simulated data are fundamental to test the algorithm (in terms of accuracy and robustness) under any operating conditions when experimental data are not available. A wide simulation campaign has been carried out to test the algorithm performances, obtaining promising results. In the near future, the proposed approach will be validated through suitable data coming from experimental tests organized in collaboration with Ansaldo STS and ECM SpA, which are the industrial partners of this research project.**

***Index Terms*—Weigh-in-motion systems, multibody modeling of railway vehicles, flexible multibody modeling of railway tracks.**

I. Introduction

NOWADAYS, the volume of freight transportation on railway vehicles is continuously increasing due to the fast growth of industry and commerce. Furthermore, the strong competition between transport modes and companies has enlarged the number of heavy fully loaded operating vehicles. In this context, an accurate estimation of the axle loads and a correct detection of overloads, imbalances and defects [1], [2] represent a primary concern for railways management companies, because they are strictly related to traffic safety and planning of the track maintenance. For these reasons, an increasing interest is focused (both in the railway industry and in the scientific community [3]–[6]) on the development of intelligent Weigh-in-Motion (WIM) systems [7], [8], able to automatically and efficiently estimate the axle loads while the trains are running on the track (without stopping or slowing down the vehicles).

The main goal of this work is the development of a new approach to estimate axle and wheel loads on railway vehicles at high vehicle speeds: the proposed WIM algorithm is able to estimate the loads starting from different physical input quantities **T** measured on the track, i.e. vertical forces on the sleepers [9], [10], rail shear [11]–[14] and rail bending [15], [16]. Consequently, it can be employed in different kinds of measurement stations. In the specific case study, the vertical forces on the sleepers F_z have been considered.

The vertical loads on the train axle and wheels and the possible imbalances are computedfromthe track measurements according to the assumption that the effects of the single loads (related to the single wheels) on the track are superimposable. In other words, the system is considered approximately linear with respect to the single wheel loads and each wheel load is supposed not to be influenced by the adjacent ones. This way, the global track response can be approximated as a weighted linear combination of the effects due to the single wheel loads moving on the track (see Fig. 7). Finally, to minimize the approximation error in reproducing the global track response through the combination of single loads, the WIM algorithm makes use of procedures based on least square optimization techniques. This kind of techniques has been successfully employed in similar applications, providing accurate and robust results. More particularly, O'Brien *et al.* used the least square optimization in different bridge weighing in motion applications: in [17] O'Brien *et al.* applied these techniques to identify the moving loads acting on the bridge starting from the measured bridge responses, while in [18]–[20] this method is exploited to improve the performance of a bridge weighing in motion system in estimating the axle loads.

The second aim of the new proposed algorithm is the accurate estimation of the unbalanced wheel loads to prevent dangerous vehicle imbalances. Starting from the estimated unbalanced wheel loads, the novel approach allows also the calculation of the vehicle center of gravity.

To achieve the previous goals, the algorithm exploits an accurate flexible multibody model of the track, taking into account the stiffness of rails, sleepers and ballast.

The algorithm can receive as inputs both experimental data and simulated ones, fundamentalto test the algorithm under any

Manuscript received March 17, 2015; revised May 30, 2015 and July 27, 2015; accepted September 4, 2015. Date of publication September 28, 2015; date of current version November 23, 2015. The Associate Editor for this paper was P. Zingaretti.

The authors are with the Department of Industrial Engineering, University of Florence, 50139 Florence, Italy (e-mail: benedetto.allotta@unifi.it; pierluca.dadamio@unifi.it; lorenzo.marini@unifi.it; enrico.meli@unifi.it; luca.pugi@unifi.it; andrea.rindi@unfi.it).

Color versions of one or more of the figures in this paper are available online at http://ieeexplore.ieee.org.

Digital Object Identifier 10.1109/TITS.2015.2477104

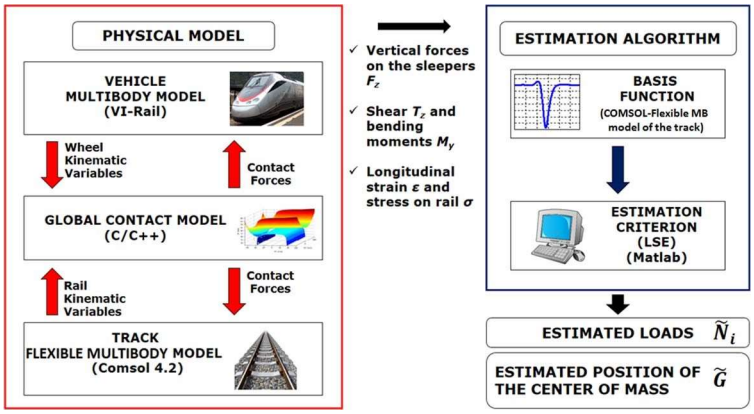

Fig. 1. General architecture of the WIM system: the flexible multibody model of the track is used both in the physical model and in the estimation algorithm to generate the basis functions.

operating conditions when experimental data are not available. To generate the simulated data, an accurate multibody model of the vehicle has been developed as well, interacting online with the track model through a global contact model developed by the authors in previous works [21], [22]. Finally, to reproduce real conditions, both physical uncertainties and measurement noise have been included into the developed model.

At this initial phase of the research activity, the performances of the innovative WIM algorithm have been tested through suitable simulation campaigns (a simplified version of the proposed algorithm was partially and preliminary validated in [6]). Such campaigns are crucial to verify the algorithm accuracy and robustness under different operating conditions, including the most critical ones, when experimental data are not available. In particular the model is tested by varying the mass M of the vehicle car-body and the vehicle speed V and, subsequently, by varying the position of center of mass G and the speed V.

The proposed estimation architecture showed a good accuracy under any operative conditions and provided promising results also in presence of quite high vehicle speeds and measurement noise. Concerning the future developments, more exhaustive experimental tests are scheduled by Ansaldo STS and ECM Spa, considering different wagon geometries and train compositions.

II. General Architecture of the Model

The general architecture of the *Weigh-in-Motion* (WIM) system is represented in Fig. 1. The architecture is composed of two parts: the physical model and the estimation algorithm. The generic inputs of the estimation algorithm **T** can be of two types: experimental data related to the railway track or, in absence of them, simulated data. In this second case, the necessary track inputs are provided by the physical model through numerical simulations of the vehicle moving on the track. The required simulations are performed to obtain the dynamic response of the track and take into account the measurement chain and the noise sources.

The physical model (Fig. 1) of the railway track consists of two sub-systems:

- the 3D multibody model of the vehicle, implementedusing the ADAMS VI-Rail software;
- the 3D flexible multibody model of the railway track,developed in the Comsol environment ([23], [24]).

The two models interact to each other during the simulation through a global wheel-rail contact model developed by the authors in previous works [22].

At each time integration step, the vehicle multibody model evaluates the kinematic variables (position,orientationand their derivatives) of each wheel. At the same time, the flexible multibody model of the railway track calculates position, orientation and their derivatives for each node/point of the beam modeling the rail. Both the kinematic variables are then sent as inputs to the global wheel-rail contact model that evaluates the global contact forces to be applied to vehicle and track.

The estimation part of the system (see Figs. 1 and 2) is composed of the innovative WIM algorithm to estimate the vertical loads on the wheels (implemented in Matlab environment) and the flexible multibody model of the track, used to generate the elementary solutions related to the single wheel loads moving on the track (see Fig. 7). This set of solutions (one for each wheel load) can be considered as a basis of functions. More precisely, each element of this function basis is the solution obtained considering only a single wheel load moving along the track (associated to a single wheel).

The measured input signal **T** is approximated as a linear combination of the basis functions (associated to the single wheel loads), thanks to the assumption that the system is approximately linear with respect to the single wheel loads and the effects of the single wheel loads on the track are superimposable (see Fig. 7). This way, the estimated loads will be proportional to the coefficients of the linear combination.

In order to minimize the estimation error in reproducing the global track response through the combination of the single load solutions contained into the function basis, the WIM algorithm makes use of least square optimization techniques ([25]–[27]).

During the estimation, some additional information is required concerning the vehicle speed V, the axle number n_{tot} and the axle positions along the railway vehicle x_{ai} with i = 1,...,n_{tot}. These further physical quantities can be measured through additional sensors or transmitted by the vehicle by means of low cost technologies.

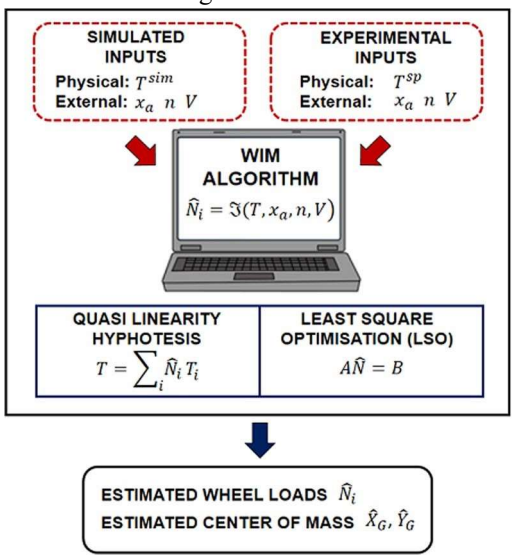

Fig. 2. WIM algorithm: the estimation makes use of the flexible multibody model of the track to generate the basis functions.

Starting from the knowledge of the track measured inputs **T** (in the case study the vertical forces on the sleepers F_z) and of V, n_{tot}, x_{ai}, the WIM algorithm estimates both the wheel and axle loads N, and the longitudinal $\widehat{X}_G$ and lateral $\widehat{Y}_G$ position of the vehicle center of mass G. The developed WIM algorithm is able to estimate the above-mentioned quantities even if the wheel load distribution is highly asymmetric.

III. Physical Model of the Railway Track

In order to perform suitable simulation campaigns to test the WIM algorithm when experimental data are not provided, a model involving all the components of the track infrastructure and of the vehicle is required. An accurate model of the track is also required to build the basis functions used by the estimation algorithm. The physical model of the system consists of a 3D flexible multibody model of the infrastructure (including rail, sleepers and ballast), a 3D multibody model of the vehicle and a wheel-rail contact model describing the interaction between the vehicle wheels and the rails. The vehicle model and the infrastructure model interact online during the simulations by means of the 3D global contact model, specifically developed to improve the reliability and the accuracy of the contact points detection. In particular, the adopted contact model is based on a two step procedure: the contact points detection [21], [22] and the global contact forces evaluation [11].

In the rest of the paper the generic vertical right and wheel loads will be indicated as $\widehat{N}_{Ri}$ and $\widehat{N}_{Li}$. The corresponding estimated quantities N_{Ri} and N_{Li} will be computed by the presented WIM algorithm.

A. The Infrastructure Model

Rail and infrastructures are modelled as 3D beams (discretized through BEAM elements with two nodes for element and 6 DOFs for each node; see Fig. 3), supported by an elastic discrete foundation representing sleepers and ballast. The rails are connected through visco-elastic elements to n_{sl} 2D rigid

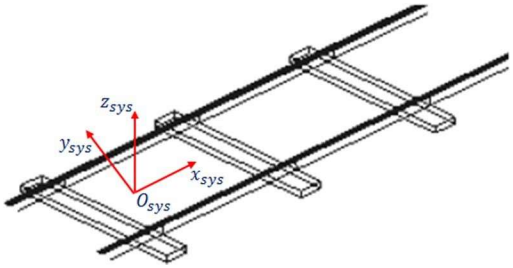

Fig. 3. Fixed reference system and rails.

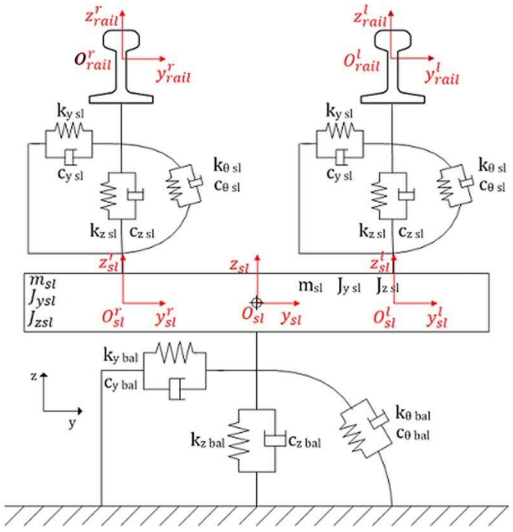

Fig. 4. Model of the interaction among rails, sleeper and ballast.

bodies representing the sleepers, which are in turn supported by a visco-elastic foundation including the ballast properties (see Fig. 4). The discretized equation of the rail is defined as:

$$M\ddot{\mathbf{q}}^{\frac{l}{r}} + C\dot{\mathbf{q}}^{\frac{l}{r}} + K\mathbf{q}^{\frac{l}{r}} = \mathbf{F}^{\frac{l}{r}} \quad (1)$$

in which M, C and K are the mass, damping and stiffness matrices of the rail, $\mathbf{q}^{l/r}$ are the discretized rail displacements and $\mathbf{F}^{l/r}$ are the applied external forces:

$$\mathbf{F}_r = \mathbf{F}_{\mathbf{sl}r} + \mathbf{F}_{\mathbf{c}r} + \mathbf{F}_{\mathbf{f}r} \quad (2)$$

where $\mathbf{F}^{l/r}_{\mathbf{sl}}$, $\mathbf{F}^{l/r}_{\mathbf{c}}$ and $\mathbf{F}^{l/r}_{\mathbf{b}}$ are, respectively, the sleeper forces, the contact forces (provided the wheel-rail contact model and to be considered if the model is used to simulate the vehicle and track dynamics) and the forces due to the crossing of the single wheel loads along the track (to be considered if the model is

used to build the basis functions required by the estimation algorithm). In other words, both the contact forces

$\mathbf{F}^{l/r}_{\mathbf{c}}$ and the single wheel loads $\mathbf{F}^{l/r}_{\mathbf{b}}$ are loads moving along the rail applied to the 3D rail beams. Since the rail beams are connected to all the sleeper-ballast systems through suitable visco-elastic elements, the moving wheel loads influence all the sleepers (especially the ones near to the positions of the loads). If the complete system dynamics (track and vehicle) is studied, the wheel loads $\mathbf{F}^{l/r}_{\mathbf{c}}$ moving on the track are provided by the wheel-rail contact model used to describe the vehicletrack interaction. Otherwise, if the track responses to the single wheel loads have to be calculated to evaluate the basis functions (used into the estimation algorithm),the wheel loads moving on the track are just the single wheel loads $\mathbf{F}^{l/r}_{\mathbf{b}}$.

The variables related to the generic node $\mathbf{q}^{l/r}_{\mathbf{i}} \in R^6$ are the linear displacements $\mathbf{v} \in R^3$ and the rotational displacements $\theta \in R^3$:

$$\mathbf{q}^{\frac{l}{r}}_{\mathbf{i}} = \begin{bmatrix} \mathbf{v}^{\frac{l}{r}}_{\mathbf{i}} \\ \boldsymbol{\theta}^{\frac{l}{r}}_{\mathbf{i}} \end{bmatrix} \tag{3}$$

where the vector $\mathbf{v}_{\mathbf{i}}{}^{l/r}$ includes longitudinal $u^{l/r}{}_{i\text{rail}}$, lateral $v_i{}^{l/r}{}_{\text{rail}}$ and vertical $w^{l/r}_{i_{\text{rail}}}$ displacements expressed in the fixed reference system $O_{\text{sys}}x_{\text{sys}}y_{\text{sys}}z_{\text{sys}}$. The vector $\theta^{l/r}_{\mathbf{i}}$ comprises the rotational displacements $\phi^{l/r}_{i_{\text{rail}}}$, $\theta^{l/r}_{i_{\text{rail}}}$ and $\psi^{l/r}_{i_{\text{rail}}}$ expressed in the fixed reference system $O_{\text{sys}}x_{\text{sys}}y_{\text{sys}}z_{\text{sys}}$ (see Fig. 3).

In this work the structural damping of the rail is modelled using the "proportional" or Rayleigh damping; the damping matrix $\mathbf{C}$ is evaluated as a linear combination of the inertia $\mathbf{M}$ and stiffness $\mathbf{K}$ matrices of the structure:

$$\mathbf{C} = \alpha_r\mathbf{M} + \beta_r\mathbf{K}. \tag{4}$$

The coefficients α_r and β_r are calibrated to fit the typical rail dynamical behavior expected from experimental results and physical considerationsavailable in the literature [3], [28], [29].

In this work the UIC60 rail profile (with cant angle equal to 1/20) has been adopted. The main physical characteristics of the rail beam model are reported in [9]. The length of the straight track section studied in the work is L = 72 m and the separation distance between two adjacent sleepers is equal to l = 0.60 m. The sleepers are modelled as 2D rigid bodies connected to the rails by means of visco-elastic elements including lateral k_{ysl}, vertical k_{zsl} and rotational $k_{\vartheta sl}$ stiffness and lateral c_{ysl}, vertical c_{zsl} and rotational $c_{\vartheta sl}$ damping properties (see Fig. 4). The longitudinal position x_{slp} along the track of the $p-$th 2D system modeling the sleepers-ballast ensemble can be expressed as follows:

$$x_{slp} = L_I + (p-1)l, \qquad k = 1,2,\ldots,n_{sl} \tag{5}$$

where $x_{sl1} = L_I$, $x_{slnsl} = L_F$ (L_I and L_F are the beginning and the end of the straight track respectively)and n_{sl} is the total number of sleepers.

The generic 2D sleeper is supported by a flexible foundation: the behavior of the ballast is characterized through the lateral $k_{y\text{bal}}$, vertical $k_{z\text{bal}}$ and rotational $k_{\vartheta\text{ball}}$ stiffness and through lateral $c_{y\text{bal}}$, vertical $c_{z\text{bal}}$ and rotational $c_{\vartheta\text{bal}}$ damping (see Fig. 4). The 3DOF bodymodelingthe sleepers-ballastensemble is described by the lateral y_{sl} and vertical z_{sl} translations and the rotation ϑ_{sl} around the $x_{sl}-$ axis of the sleeper reference system (all expressed in the reference system $O_{\text{sys}}x_{\text{sys}}y_{\text{sys}}z_{\text{sys}}$ (see Fig. 4)).

At this point, the dynamic model of the sleeper can be expressed through the following equation:

$$\begin{aligned} &M_{sl}\ddot{\mathbf{v}}^{p}_{sl} + K_{sl}\left(\mathbf{v}^{pr}_{sl} - \mathbf{v}^{pr}_{\text{rail}}\right) \\ &\quad + \mathrm{C}_{sl}\left(\dot{\mathbf{v}}^{pr}_{sl} - \dot{\mathbf{v}}^{pr}_{\text{rail}}\right) + K_{sl}\left(\mathbf{v}^{pl}_{sl} - \mathbf{v}^{pl}_{\text{rail}}\right) \\ &\quad + \mathrm{C}_{sl}\left(\dot{\mathbf{v}}_{slpl} - \dot{\mathbf{v}}_{\text{rail}\,pl}\right) + K_{\text{bal}}\mathbf{v}_{slp} + \mathrm{C}_{\text{bal}}\dot{\mathbf{v}}_{slp} = 0 \end{aligned} \tag{6}$$

where the subscript sl refers to the sleeper, the subscript bal is related to the ballast quantities, the subscript rail refers to the rails and l/r is related to the left and right sides of the track. The vector $\mathbf{v}_{sl}{}^{p}$ includes the lateral v^{p}_{sl}, vertical w^{p}_{sl} and rotational ϕ^{p}_{sl}displacements of the sleeper expressed in the fixed reference system $O_{\text{sys}}x_{\text{sys}}y_{\text{sys}}z_{\text{sys}}$ (see Fig. 4); M_{sl} is the sleeper mass matrix while K_{sl} and C_{sl} are respectively the stiffness and damping matrices characterizing the rail-sleeper visco-elastic connection. The K_{bal} and C_{bal} are respectively the stiffness and damping matrices of the ballast. The vectors $\mathbf{v}_{sl}{}^{pl}$, $\mathbf{v}_{sl}{}^{pr}$ are defined as:

$$\mathbf{v}^{pr}_{sl} = \begin{pmatrix} v^{pr}_{sl} \\ w^{pr}_{sl} \\ \phi^{pr}_{sl} \end{pmatrix} = \begin{bmatrix} v^{p}_{sl} \\ w^{p}_{sl} - \phi^{p}_{sl}\frac{s}{2} \\ \phi^{p}_{sl} \end{bmatrix} \tag{7}$$

$$\mathbf{v}^{pl}_{sl} = \begin{pmatrix} v^{pl}_{sl} \\ w^{pl}_{sl} \\ \phi^{pl}_{sl} \end{pmatrix} = \begin{bmatrix} v^{p}_{sl} \\ w^{p}_{sl} + \phi^{p}_{sl}\frac{s}{2} \\ \phi^{p}_{sl} \end{bmatrix} \tag{8}$$

where s indicates the railway gauge between the rails. The vectors $\mathbf{v}^{pl}_{\text{rail}}$, $\mathbf{v}^{pr}_{\text{rail}}$ are defined as:

$$\mathbf{v}^{pr}_{\text{rail}} = \begin{bmatrix} v^{pr}_{\text{rail}} \\ w^{pr}_{\text{rail}} \\ \phi^{pr}_{\text{rail}} \end{bmatrix} \quad \mathbf{v}^{pl}_{\text{rail}} = \begin{bmatrix} v^{pl}_{\text{rail}} \\ w^{pl}_{\text{rail}} \\ \phi^{pl}_{\text{rail}} \end{bmatrix}. \tag{9}$$

The main physical quantities related to the sleepers-ballast system can be found in [6].

B. The Vehicle Model

The railway vehicle chosen for the dynamic simulations is the Manchester Wagon, the geometric and mechanical characteristics of the wagon are easily available in the literature [30]. The 3D multibody model of this vehicle has been widely studied and validated under different operating conditions. The

model of the Manchester Wagon, implemented in the Adams VI-Rail environment, consists of seven rigid bodies (one car body, two bogies and four wheelsets). The rigid bodies are connected by means of appropriate elastic and damping elements; more particularly, the vehicle is equipped with two suspension stages. The primary suspensions connect the wheelsets to the bogies and comprise two coil springs and six dampers (longitudinal, lateral and vertical ones), while the secondary suspensions connect the bogies to the coach and consist of the following elements:

- two coil springs;
- four dampers (lateral and vertical ones);
- the traction rod;
- the roll bar;• two lateral bumpstops.

Both the suspension stages have been modelled by means of three-dimensional nonlinear force elements like bushings, dampers, and bumpstops [31]. In this work the ORE S1002 profile has been used for the wheel profiles.

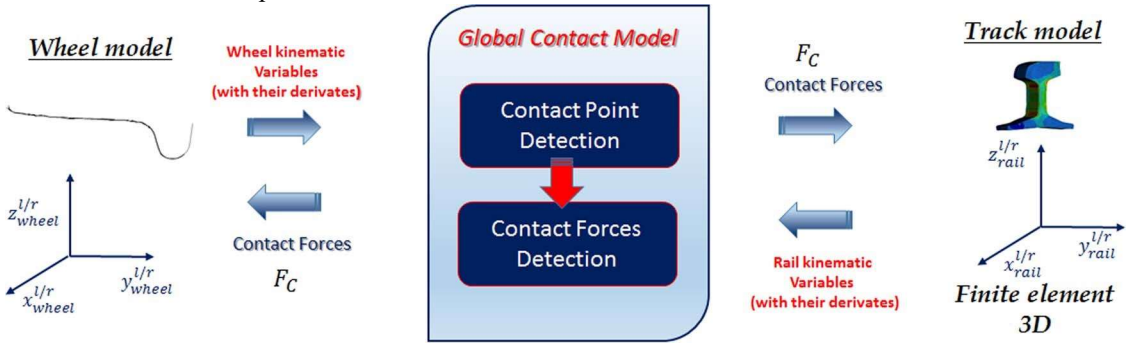

Fig. 5. Global contact model: interaction between the multibody vehicle model and the flexible model of the track.

C. Global Contact Model

The vehicle model and the infrastructure model interact online during the simulation by means of a 3D global contact model developed by the authors in previous works to improve the reliability and the accuracy of the contact points detection (see Fig. 5). In particular, the global contact model comprises both an innovative contact points detection algorithm [21], [22] and the contact forces evaluation part [11]. The vehicle and infrastructure models calculate the wheel kinematic variables (related to each wheel) and the rail kinematic variables (related to each rail node). Starting from these quantities, the global contact model evaluates the contact forces to be applied to the wheel and the rail.

D. Measurement Error

To improve the accuracy of the physical model of the railway track (infrastructure and vehicle model), the following disturbances on the generic measured input **T** (in this work the vertical forces on the sleepers F_z) have been considered:

- *frequency effects on the input signals* $\mathbf{T}_r$, $\mathbf{T}_l$ *due to the limited band of physical system and measurement chain*: the frequency effects due to the limited band of the real system and the rail measurement chain have been modelled through a second order low pass filter directly applied to the simulated signals $\mathbf{T}^{sim}_{rk}$, $\mathbf{T}^{sim}_{lk}$ related to the k-th measure points x_{rk} and x_{lk} of the measurement station (where $k = 1,\ldots N_m$ and r, l are referred to the right and left track sides):

$$\mathbf{T}_{frk}(t) = B_{2,\omega_n}(s)\mathbf{T}_{simrk}(t), \mathbf{T}_{flk}(t) = B_{2,\omega_n}(s)\mathbf{T}_{simlk}(t) \quad (10)$$

in which $B_{2,\omega_n}(s)$ is the second order Butterworth filter and $\omega_n = 2\pi f_n$ is the cut frequency (ω_n in rad/s and f_n in **Hz**). • *numerical disturbances and bias errors on the signal* $\mathbf{T}^f_{rk}, \mathbf{T}^f_{lk}$: besides the frequency effects, also numerical disturbances and bias errors on the signals $\mathbf{T}^f_{rk}, \mathbf{T}^f_{lk}$ have been modelled:

$$\mathbf{T}^{fn}_{rk}(t) = \mathbf{T}^f_{rk}(t) + U_{T_r}\left[\mu_{T_r}, \delta_{\frac{T_r}{2}}\right] \quad (11)$$

$$\mathbf{T}_{fnlk}(t) = \mathbf{T}_{flk}(t) + U_{Tl}\left[\mu_{T_l}, \delta_{\frac{T_l}{2}}\right] \quad (12)$$

where μ_{Tr}, μ_{Tl} and $\delta_{Tl/2}, \delta_{Tr/2}$ are the mean and the variance of the disturbance distribution U_{Tr}, U_{Tr}. The aim

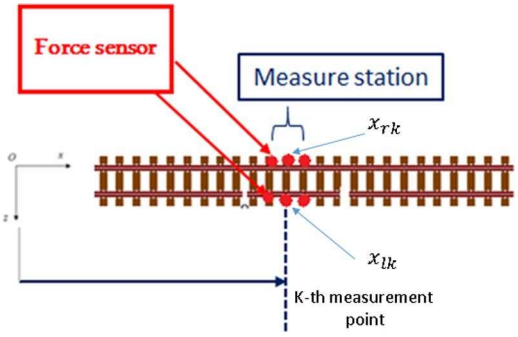

Fig. 6. Measurement layout.

of numerical disturbances and bias errors on the signals $\mathbf{T}^{fn}_{rk}, \mathbf{T}^{fn}_{lk}$ is to properly reproduce the numerical noise affecting the measurement; therefore they have to be applied to the signals only after the low pass filter.

The measurement errors will play a fundamental role when the physical model of the railway track is employed to test the accuracy and the robustness of the WIM algorithm in absence of experimental data.

IV. WIM Algorithm

In this chapter the innovative WIM algorithm for the estimation of the vertical wheel loads $\widehat{N}_{Ri}$ and $\widehat{N}_{Li}$ with i = 1,...,n_{tot} on railway vehicles is described. The nominal values of the loads N_{Ri} and N_{Li} are taken from the model in the simulated case, or are the nominal wheel load values in the experimental case. As previously stated, the WIM system presented in the current paper is based on the measurements of the vertical forces F_z acting on the sleepers, acquired by means of dedicated force sensitive elements placed over the sleepers in the sections corresponding to the rail baseplate. The WIM system consists of various measure points (few if possible to reduce both measure station dimensions and costs) placed along the railway track (see Fig. 6).

A. Architecture of the WIM Algorithm

The general architecture of the system is described in the diagram in Fig. 2. The developed WIM algorithm performs the estimation of the actual vertical right $\widehat{N}_{Ri}$ and left $\widehat{N}_{Li}$ wheel loads starting from the generic track measurements chosen as input signals $\mathbf{T}_{rk}$ and $\mathbf{T}_{lk}$ (with k = 1,..,N_m), measured respectively at x_{rk} and x_{lk} (the right and left abscissas of the k−th measurement point (see Fig. 6)).

The main idea behind the new WIM algorithm arises from the quite intuitive hypothesis that the system is approximately linear with respect to the vertical loads N_{Ri}, N_{Li} with i = 1,...,n_{tot} (the so-called *quasi-linearity hypothesis* (QLH)). In other words, the effect of the generic load N_{Ri} and N_{Li} on the generic track measurementinput $\mathbf{T}_{rk}$ and $\mathbf{T}_{lk}$ (in the case study the vertical forces on the sleepers F_{zrk} and F_{zlk}) is assumed not to be affected by the presence of other loads (especially the adjacent ones). Of course, in order to properly apply the superposition principle, the *quasi-linearity hypothesis* (QLH) must hold within the whole range of considered velocities V and cut frequencies f_n. Thanks to the previous assumption, the application of the superposition principle allows the calculation of the track inputs $\mathbf{T}_{rk}$ and $\mathbf{T}_{lk}$. More specifically, the track inputs $\mathbf{T}_{rk}$ and $\mathbf{T}_{lk}$ are approximated through a linear combination of $2n_{tot}$ track input signals (namely the basis functions) produced by $2n_{tot}$ single wheel loads N_f (one for each vehicle wheel): the single wheel loads movealong the track at the speed V and are properly shifted in the time of a delay t_i to exactly follow the i−th wheel (see chapter IV-B and Fig. 7). In order to calculate this basis, the algorithm makes use of the flexible multibody model of the track described in Par. III-A. The linear and will allow the easy calculation of $N_{Ri}$and N_{Li}. combination coefficients will be equal to N_{Ri}/N_f and N_{Li}/N_f

Obviously, since the system is only approximately linear, a *Least Squares Optimization* (LQSO) is needed to minimize the approximation error and, at the same time, to optimize the values of $\widehat{N}_{Ri}$ and $\widehat{N}_{Li}$.

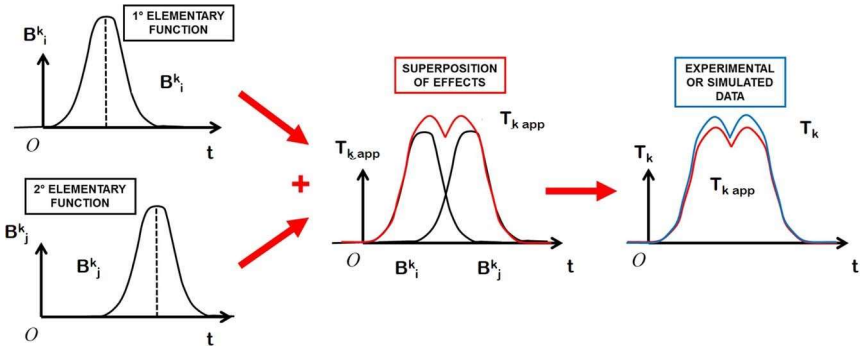

Fig. 7. Schematic representation of the quasi-linearity hypothesis.

B. The Quasi-Linearity Hypothesis

As previously stated, if the *quasi-linearity hypothesis* (QLH) holds, the application of the superposition effects allows the approximation of the right $\mathbf{T}_{rk}$ and left $\mathbf{T}_{lk}$ track inputs produced by the transit of the entire vehicle through a linear combination of track responses (namely the basis functions) produced by single wheel loads N_f (see for example Fig. 7). The presented WIM algorithm takes into account the coupling effect between the left and the right rail deformations caused by the dynamical behavior of the sleeper-ballast ensemble. For this reason, in the most general version of the WIM algorithm, the function basis must include the responses to the transit of both the left and the right single wheel loads.

More specifically, the quantities $\mathbf{B}^{rk}_{Ri}$ and $\mathbf{B}^{rk}_{Li}$ represent the track responses to the transit of the i−th single wheel load respectively on the right and on the left rail (subscripts R and L), measured at the right (r) side of the k−th measurement point.

Analogously, $\mathbf{B}^{lk}_{Ri}$ and $\mathbf{B}^{lk}_{Li}$ are the track responses to the transit of the i−th single wheel load respectively on the right and on the left rail, measured at the left (l) side of the k−th measurement station. At this preliminary phase of the research activity, the model of the rail infrastructure used to evaluate the basis function is analogous to the one adopted to simulate the whole physical system (described in SectionIII and III-A), except for the effects due to noise and limited band, inserted to make the complete physical model more realistic. All the $2n_{tot}$ right-sidesingle load responses $\mathbf{B}^{rk}_{Ri}$ and $\mathbf{B}^{rk}_{Li}$ and the $2n_{tot}$ leftside single load responses $\mathbf{B}^{lk}_{Ri}$ and $\mathbf{B}^{lk}_{Li}$ (with i = 1,..,n_{tot} and k = 1,..,N_m) produced by the $2n_{tot}$ single wheel loads N_f (with initial position x_{af}) can be efficiently assessed by introducing suitable time delays t_i:

$$t_i = \frac{x_{ai} - x_{af}}{V} \tag{13}$$

and by applying such delays to the single load responses to the transit of a unique single load $\mathbf{B}^{r/l}_{R/L\,k}(t)$ previously calculated:

$$\mathbf{B}^{rk}_{Ri}(t) = \mathbf{B}^{rk}_{R}(t + t_i) \quad (14)$$

$$\mathbf{B}^{rk}_{Li}(t) = \mathbf{B}^{rk}_{L}(t + t_i) \quad (15)$$

$$\mathbf{B}_{lkRi}(t) = \mathbf{B}_{lkR}(t + t_i) \quad (16)$$

$$\mathbf{B}_{lkLi}(t) = \mathbf{B}_{lkL}(t + t_i) \quad (17)$$

where $t \in [T_I, T_F - t_i]$.

At this point, thanks to the superposition principle, the generic track inputs $\mathbf{T}_{rk}$, $\mathbf{T}_{lk}$ produced by the transit of the entire train can be approximated according to the following expressions:

$$\mathbf{T}^{rk}(t) \approx \mathbf{T}_{rk\,\mathrm{app}}(t) = \sum_{i=1}^{n_{\mathrm{tot}}} \mathbf{B}^{rk}_{Ri}\alpha_{Ri} + \sum_{i=1}^{n_{\mathrm{tot}}} \mathbf{B}_{rkLi}\alpha_{Li} \quad (18)$$

$$\mathbf{T}^{lk}(t) \approx \mathbf{T}_{lk\,\mathrm{app}}(t) = \sum_{i=1}^{n_{\mathrm{tot}}} \mathbf{B}_{lkRi}\alpha_{Ri} + \sum_{i=1}^{n_{\mathrm{tot}}} \mathbf{B}_{lkLi}\alpha_{Li} \quad (19)$$

where the linear combination coefficients α_{Ri}, α_{Li}, the estimated vertical loads $\widehat{N}_{Ri}$, $\widehat{N}_{Li}$ and the single wheel vertical load N_f are connected by the following expressions:

$$\alpha_{Ri} = \frac{\widehat{N}_{Ri}}{N_{Rf}}, \quad \alpha_{Li} = \frac{\widehat{N}_{Li}}{N_{Lf}} \quad (20)$$

C. Least Squares Estimation

Since the studied system is only approximately linear, a *Least Squares Optimization* (LSO) is necessary to minimize the approximationerror between $\mathbf{T}_{rk}$, $\mathbf{T}_{lk}$ and $\mathbf{T}^{rk}_{\mathrm{app}}$, $\mathbf{T}_{lk\,\mathrm{app}}$ and, at the same time, to optimize the values of N_{Ri}, N_{Li}. In this specific case, linear not-weighted least squares have been considered [25]–[27].

In the present research activity the vertical forces acting on the sleepers F_{zrk} and F_{zlk} have been considered as track inputs. Consequently, equations (18) and (19) become:

$$F_{z\,rk}(t) \approx \sum_{i=1}^{n_{\mathrm{tot}}} \alpha^{\mathrm{sim}}_{Ri} B^{rk}_{Ri}(t) + \sum_{i=1}^{n_{\mathrm{tot}}} \alpha^{\mathrm{sim}}_{Li} B^{rk}_{Li}(t) \quad (21)$$

$$F_{z\,lk}(t) \approx \sum_{i=1}^{n_{\mathrm{tot}}} \alpha^{\mathrm{sim}}_{Ri} B^{lk}_{Ri}(t) + \sum_{i=1}^{n_{\mathrm{tot}}} \alpha^{\mathrm{sim}}_{Li} B^{lk}_{Li}(t) \quad (22)$$

with $k = 1, 2, \ldots, N_m$. Furthermore, to simulate the sampling due to the measurement process, the time domain $t \in [T_I, T_F - t_i]$ has been discretized with a sample time equal to $\Delta t = 0.001$ s. Therefore, the track inputs F_{zrk} and F_{zlk} and the single wheel load responses $B_{Ri}{}^{rk}$, $B_{Li}{}^{rk}$, $B_{Ri}{}^{lk}$, $B_{Li}{}^{lk}$ (in this case forces too) are known only at the times t_h with $h = 1, 2, \ldots n_s$ (n_s is the sample number). The following discretized expressions hold for F_{zrk} and F_{zlk}:

$$\mathbf{F}_{Dz\,rk} = \begin{bmatrix} F_{z\,rk}(t_1) \\ \vdots \\ F_{z\,rk}(t_{n_s}) \end{bmatrix}, \quad \mathbf{F}_{Dz\,lk} = \begin{bmatrix} F_{z\,lk}(t_1) \\ \vdots \\ F_{z\,lk}(t_{n_s}) \end{bmatrix} \quad (23)$$

The same time discretization can be considered also for the single wheel load responses $B_{Ri}{}^{rk}$, $B_{Li}{}^{rk}$, $B_{Ri}{}^{lk}$, $B_{Li}{}^{lk}$ employed to estimate F_{zrk} and F_{zlk}:

$$\mathbf{B}^{rk}_{DRi} = \left[B^{rk}_{Ri}(t_1) \ldots B^{rk}_{Ri}(t_h) \ldots B^{rk}_{Ri}(t_{n_s})\right]^T \quad (24)$$

$$\mathbf{B}^{rk}_{DLi} = \left[B^{rk}_{Li}(t_1) \ldots B^{rk}_{Li}(t_h) \ldots B^{rk}_{Li}(t_{n_s})\right]^T \quad (25)$$

$$\mathbf{B}^{lk}_{DRi} = \left[B^{lk}_{Ri}(t_1) \ldots B^{lk}_{Ri}(t_h) \ldots B^{lk}_{Ri}(t_{n_s})\right]^T \quad (26)$$

$$\mathbf{B}^{lk}_{DLi} = \left[B^{lk}_{Li}(t_1) \ldots B^{lk}_{Li}(t_h) \ldots B^{lk}_{Li}(t_{n_s})\right]^T. \quad (27)$$

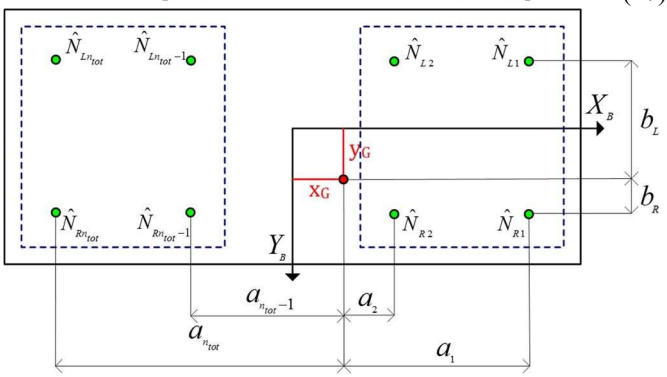

Fig. 8. Evaluation of the lateral Y_G and longitudinal X_G coordinates of the vehicle center of gravity.

Since equations (21) and (22) must hold for all the times t_h, defining the matrix $A \in \mathbb{R}^{2n_s N_m \times 2n_{\mathrm{tot}}}$ and the vector $\mathbf{b} \in \mathbb{R}^{2n_s N_m \times 1}$ in (28) and (29), shown at the bottom of the page. The discretized form of equations (21) and (22) can be obtained:

$$\mathbf{b} \simeq A\boldsymbol{\alpha}^{\mathrm{sim}} \quad (30)$$

$$\boldsymbol{\alpha}^{\mathrm{sim}} = \left[\alpha_R^{\mathrm{sim}\,T}\, \alpha_L^{\mathrm{sim}\,T}\right]^T \quad (31)$$

where

$$\boldsymbol{\alpha}^{\mathrm{sim}}_R = \left[\alpha^{\mathrm{sim}}_{R1}\alpha^{\mathrm{sim}}_{R2}\alpha^{\mathrm{sim}}_{R3}\alpha^{\mathrm{sim}}_{R4}\right]^T \quad (32)$$

$$\boldsymbol{\alpha}^{\mathrm{sim}}_L = \left[\alpha^{\mathrm{sim}}_{L1}\alpha^{\mathrm{sim}}_{L2}\alpha^{\mathrm{sim}}_{L3}\alpha^{\mathrm{sim}}_{L4}\right]^T. \quad (33)$$

By means of a *least squares optimization* (LSO) (in this case linear and not-weighted), it is now possible to minimize the

squared 2-norms $E^2 = \|\mathbf{E}\|_2^2$ of the approximation error **E** = $A\alpha^{sim}$ – **b** present in (30):

where the matrix $A^T A$ is invertible if and only if the rank of A is maximum. Finally the values of the estimated vertical loads N_{Ri},

$$\alpha_{sim} = (A_T A)^{-1} A_T \mathbf{b}_{fn} \qquad (34)$$

$$\left[\begin{array}{ccccc|ccccc}
\mathbf{B}_{DR1}^{r1} & \cdots & \mathbf{B}_{DRi}^{r1} & \cdots & \mathbf{B}_{DRn_{tot}}^{r1} & \mathbf{B}_{S1}^{r1} & \cdots & \mathbf{B}_{DLi}^{r1} & \cdots & \mathbf{B}_{DLn_{tot}}^{r1} \\
\vdots & & \vdots & & \vdots & \vdots & & \vdots & & \vdots \\
\mathbf{B}_{DR1}^{rk} & \cdots & \mathbf{B}_{DRi}^{rk} & \cdots & \mathbf{B}_{DRn_{tot}}^{rk} & \mathbf{B}_{S1}^{rk} & \cdots & \mathbf{B}_{DLi}^{rk} & \cdots & \mathbf{B}_{DLn_{tot}}^{rk} \\
\vdots & & \vdots & & \vdots & \vdots & & \vdots & & \vdots \\
\mathbf{B}_{DR1}^{rN_m} & \cdots & \mathbf{B}_{DRi}^{rN_m} & \cdots & \mathbf{B}_{DRn_{tot}}^{rN_m} & \mathbf{B}_{DL1}^{rN_m} & \cdots & \mathbf{B}_{DLi}^{rN_m} & \cdots & \mathbf{B}_{DLn_{tot}}^{rN_m} \\
\hline
\mathbf{B}_{DR1}^{l1} & \cdots & \mathbf{B}_{DRi}^{l1} & \cdots & \mathbf{B}_{DRn_{tot}}^{l1} & \mathbf{B}_{DL1}^{l1} & \cdots & \mathbf{B}_{DLi}^{l1} & \cdots & \mathbf{B}_{DLn_{tot}}^{l1} \\
\vdots & & \vdots & & \vdots & \vdots & & \vdots & & \vdots \\
\mathbf{B}_{DR1}^{lk} & \cdots & \mathbf{B}_{DRi}^{lk} & \cdots & \mathbf{B}_{DRn_{tot}}^{lk} & \mathbf{B}_{DL1}^{lk} & \cdots & \mathbf{B}_{DLi}^{lk} & \cdots & \mathbf{B}_{DLn_{tot}}^{lk} \\
\vdots & & \vdots & & \vdots & \vdots & & \vdots & & \vdots \\
\mathbf{B}_{DR1}^{lN_m} & \cdots & \mathbf{B}_{DRi}^{lN_m} & \cdots & \mathbf{B}_{DRn_{tot}}^{lN_m} & \mathbf{B}_{DL1}^{lN_m} & \cdots & \mathbf{B}_{DLi}^{lN_m} & \cdots & \mathbf{B}_{DLn_{tot}}^{lN_m}
\end{array}\right]$$

$$\begin{matrix} {}^{T}_{Dzrk} & & {}^{T}_{Dzl1} & & {}^{T} \end{matrix}$$

$$A = \qquad (28)$$

$$B$$

B

$$\mathbf{b} = \mathbf{F}_{TDzr1} \ldots \mathbf{F} \quad \ldots \mathbf{F}_{TDzrN_m} \mathbf{F} \quad \ldots \mathbf{F}_{DzlkT} \quad \ldots \mathbf{F}_{DzlNT_m} \qquad (29)$$

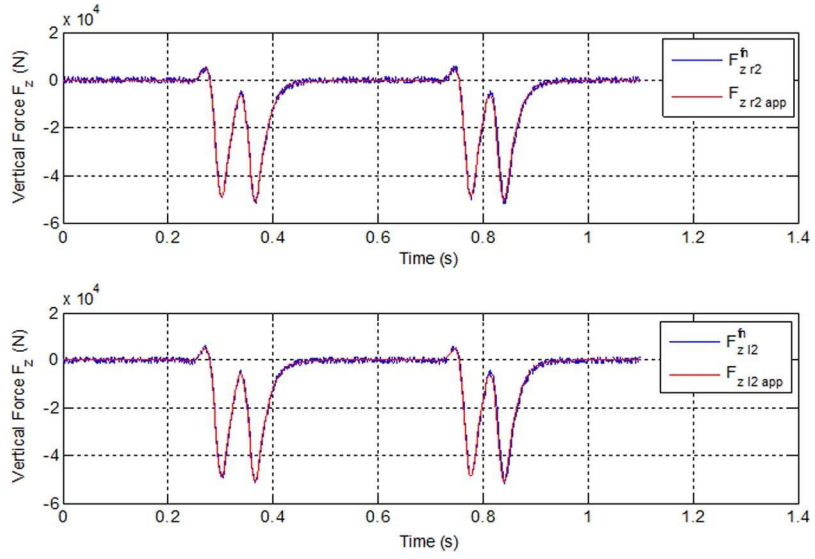

Fig. 9. Vertical forces acting on x_{r2} = 34.2; comparison between the forces calculated by the physical model $F_{zr2}(t)$, $F_{zl2}(t)$ and the ones obtained according to the *quasi-linearity hypothesis* $F_{zr2app}(t)$, $F_{zl2app}(t)$.

$\widehat{N}_{Li}$ can be computed starting from the knowledge of α^{sim}:

$$\frac{N^{\text{sim}}}{N_f} = \left[\frac{\widehat{N}_{R1}}{N_{Rf}}\frac{\widehat{N}_{R2}}{N_{Rf}}\frac{\widehat{N}_{R3}}{N_{Rf}}\frac{\widehat{N}_{R4}}{N_{Rf}}\frac{\widehat{N}_{L1}}{N_{Lf}}\frac{\widehat{N}_{L2}}{N_{Lf}}\frac{\widehat{N}_{L3}}{N_{Lf}}\frac{\widehat{N}_{L4}}{N_{Lf}}\right]^T$$

$\alpha_{\text{sim}} =$ (35)

where

$$\widehat{\mathbf{N}} = \left[\widehat{\mathbf{N}}_R^{\text{sim}\,T}\,\widehat{\mathbf{N}}_L^{\text{sim}\,T}\right]^T \tag{36}$$

with

$$\widehat{\mathbf{N}}_R = \left[\widehat{N}_{R1}\widehat{N}_{R2}\widehat{N}_{R3}\widehat{N}_{R4}\right]^T \tag{37}$$

$$\widehat{\mathbf{N}}_L = [\widehat{N}_{L1}\widehat{N}_{L2}\widehat{N}_{L3}\widehat{N}_{RL}]^T \tag{38}$$

.

D. Center of Gravity Estimation

The innovative WIM algorithm, starting from the estimated wheel loads $\widehat{N}_{Ri}$ and $\widehat{N}_{Li}$, is able to evaluate the lateral Y_G and longitudinal X_G coordinates of the vehicle center of gravity. Considering the horizontal plane containing the center of gravity (COG) of the railway vehicle and introducing the reference system Ox_By_B shown in Fig. 8 where the origin O coincides with the geometric center of the car-body, the momentum equilibrium around X_B−axis and Y_B−axis can be respectively expressed as:

$$\sum_{i=1}^{n_{\text{tot}}}(b_R\widehat{N}_{Ri} + b_L\widehat{N}_{Li}) = 0 \tag{39}$$

.

$$\sum_{i=1}^{n_{\text{tot}}} a_i(\widehat{N}_{Ri} + \widehat{N}_{Li}) = 0 \tag{40}$$

Taking into account the nominal values of the geometrical quantities of the vehicle (i.e. the longitudinal position inside the train of each axle x_{ai} and the distance between the two nominal rolling radii s), the coefficients b_R, b_L, a_i can be re-written as a function of the COG coordinates X_G, Y_G. More specifically, the following expressions hold for the coefficients b_R, b_L:

$$b_R = \frac{s}{2} - Y_G \tag{41}$$

$$b_L = -\frac{s}{2} - Y_G \tag{42}$$

whereas the coefficients a_i can be calculated as follows:

$$a_1 = -((x_{a1} - x_{a4})/2 + X_G = c1 + X_G \tag{43}$$

$$a_2 = -((x_{a2} - x_{a3})/2 + X_G = c2 + X_G \tag{44}$$

$$a_3 = ((x_{a2} - x_{a3})/2 + X_G = c3 + X_G \tag{45}$$

$$a_4 = -((x_{a1} - x_{a4})/2 + X_G = c4 + X_G. \tag{46}$$

At this point, the momentum equilibrium equations can be re-written as:

$$C\widehat{\mathbf{G}} = \mathbf{d} \tag{47}$$

where $C \in \mathbb{R}^{2\times2}$, $\widehat{\mathbf{G}}, \mathbf{d} \in \mathbb{R}^2$ and

$$\widehat{\mathbf{G}} = \begin{bmatrix}\widehat{X}_G \\ \widehat{Y}_G\end{bmatrix} = \begin{bmatrix}-\sum_{i=1}^{n_{\text{tot}}}(\widehat{N}_{Ri} + \widehat{N}_{Li})c_i \\ \sum_{i=1}^{n_{\text{tot}}}(\widehat{N}_{Li} - \widehat{N}_{Ri})\frac{s}{2}\end{bmatrix}$$

$$C = \begin{bmatrix}\sum_{i=1}^{n_{\text{tot}}}(\widehat{N}_{Ri} + \widehat{N}_{Li}) & 0 \\ 0 & \sum_{i=1}^{n_{\text{tot}}}(\widehat{N}_{Ri} + \widehat{N}_{Li})\end{bmatrix} \tag{48}$$

(49) **d**. (50)

Hence, the values of the estimated longitudinal $\widehat{X}_G$ and lateral inverting the C matrix according to the following expression: Y_G coordinates of the center of gravity G can be computed by

$$\widehat{\mathbf{G}} = C^{-1}\mathbf{d} \tag{51}$$

TABLE I
VARIATION RANGES OF V, M AND f_n ADOPTED FOR THE SIMULATIONS CAMPAIGN

Parameter	Min.	Max.	N_{sim}	Δ
Velocity ($m\,s^{-1}$)	10	40	4	$\Delta V = \frac{(V_{max} - V_{min})}{(N_{sim} - 1)}$
Car-body Mass (t)	20	50	4	$\Delta M = \frac{(M_{max} - M_{min})}{(N_{sim} - 1)}$
Frequency (s^{-1})	10	40	4	$\Delta f_n = \frac{(f_{n\,max} - f_{n\,min})}{(N_{sim} - 1)}$

V. PERFORMANCE OF THE WIM ALGORITHM

The present section describes the performance of the WIM algorithm in $\widehat{N}_{Ri}, \widehat{N}_{Li}$ estimating the vertical wheel loads(with $i = 1,\ldots,n_{\text{tot}}$), starting from the knowledge of the vertical forces acting on the sleepers F_{zrk} and F_{zlk}. More particularly, the performances of the algorithm have been evaluated in terms of accuracy by varying different parameters of the vehicle and different characteristics of the measurement chain (i.e. the vehicle car-body mass M, the vehicle speed V, the longitudinal and lateral positions of the center of gravity G and the cut-off frequency f_n of the measurement chain).

A. WIM Algorithm Performance

The basic procedure used to test the algorithm consists in comparing the nominal vertical wheel loads, N_{Ri} and N_{Li} with the estimated loads $\widehat{N}_{Ri}$ and $\widehat{N}_{Li}$ calculated by the WIM estimation algorithm. This kind of comparison is really helpful to test the algorithm accuracy when experimental data are not available. During the test campaign, the attention is focused on the estimation behavior as a function of the car-body mass M,

the vehicle speed V and the position of the center of gravity G, considering different values of the cut frequency $\hat{f}_n$.

1) Estimation of the Vertical Wheel Loads N_{Ri}, N_{Li}: Initially, by way of example, the vertical forces on the sleepers $F_{zrk}(t)=F_{zr}(x_{rk},t)$ and $F_{zlk}(t)=F_{zl}(x_{lk},t)$ simulated through the physical model of the railway track (see chapter III) are compared with the vertical forces on the sleepers $F_{zrk\text{app}}(t) = F_{zr\text{app}}(x_{rk},t)$ and $F_{zlk\text{app}}(t) = F_{zl\text{app}}(x_{lk},t)$ estimated by means of the WIM algorithm. At this phase of the research activity, the layout of the measurement station consists of three measurement points ($N_m = 3$) on both the rail sides ($x_{R1} = x_{L1} =$ 33 m, $x_{R2} = x_{L2} = 34.2$ m and $x_{R3} = x_{L3} = 38.4$ m). Fig. 9 shows both the simulated $F_{zr2}(t)$, $F_{zl2}(t)$ and the approximated $F_{zr2\text{app}}(t)$, $F_{zl2\text{app}}(t)$ right and left vertical forces acting on the second measurement point ($x_{r2} = 34.2$ m) related to a simulation performed at a speed value $V = 40$ ms^{-1}, a car-body mass $M = 50$ t and a cut frequency $f_n = 20$ Hz. The comparison highlights a good agreement between simulated and estimated quantities, confirming the accuracy of the *WIM* algorithm.

To compare the nominal N_{Ri}, N_{Li} and estimated $\hat{N}_{Ri}$, $\hat{N}_{Li}$ vertical loads on the wheels, an extensive simulations campaign has been carried out. In particular, the dependence of the relative errors $e_{Ri}^{\text{sim}} = (\widehat{N}_{Ri}^{\text{sim}} - N_{Ri})/N_{Ri}$ and $e^{\text{sim}}{}_{Li} = (\widehat{N}_{Li}^{\text{sim}} - N_{Li})/N_{Li}$ on the vehicle car-body mass M, the vehicle speed V and the cut frequency f_n of the measurement chain is investigated.In Table I the considered variation ranges for the previous quantities are reported together with the resolutions adopted for the range discretization (ΔV, ΔM, Δf_n), where N_{sim} represents the number of simulated values of M, V and f_n.

TABLE II

ESTIMATED VERTICAL LOADS ON THE VEHICLE WHEELS, $\widehat{N}_{Ri}^{\text{sim}}$, $\widehat{N}_{Li}^{\text{sim}}$: V = 40 ms^{-1}, M = 50 t, WITH DIFFERENT VALUES OF f_n

Cut frequency f_n Hz	Parameter	Value kN	Parameter	Value %
10	$\widehat{N}_{R1}^{sim}$	75.4	e_{R1}^{sim}	1.4%
20		76.4		0.3%
30		76.4		0.3%
40		76.8		0.2%
10	$\widehat{N}_{L1}^{sim}$	75.4	e_{L1}^{sim}	1.7%
20		76.5		0.2%
30		76.6		0.01%
40		76.7		0.03%
10	$\widehat{N}_{R2}^{sim}$	75.9	e_{R2}^{sim}	0.7%
20		76.6		0.05%
30		76.6		0.1%
40		76.7		0.2%
10	$\widehat{N}_{L2}^{sim}$	76.2	e_{L2}^{sim}	0.4%
20		76.2		0.4%
30		76.4		0.17%
40		76.1		0.5%
10	$\widehat{N}_{R3}^{sim}$	75.2	e_{R3}^{sim}	1.7%
20		76.2		0.5%
30		76.4		0.19%
40		76.4		0.2%
10	$\widehat{N}_{L3}^{sim}$	75.1	e_{L3}^{sim}	1.9%
20		76.2		0.4%
30		76.2		0.01%
40		76.5		0.4%
10	$\widehat{N}_{R4}^{sim}$	75.3	e_{R4}^{sim}	1.7%
20		76.2		0.6%
30		76.9		0.3%
40		76.8		0.1%
10	$\widehat{N}_{L4}^{sim}$	75.7	e_{L4}^{sim}	1.3%
20		76.6		0.1%
30		76.7		0.06%
40		76.7		0.06%

The global performances of the *WIM* algorithm have been studied by considering the maximum relative error $e_{\max}^{\text{sim}}(V, M, f_n)$:

$$e_{\max}^{\text{sim}} = \max_{1\le i\le n_{\text{tot}},} \left(\max\left(\left|e_{Ri}^{\text{sim}}\right|, \left|e_{Li}^{\text{sim}}\right.\right.\right. \quad (52)$$

The values of the nominal N_{Ri}^{sim}, N_{Li}^{sim} and estimated $\widehat{N}_{Ri}^{\text{sim}}$, $\widehat{N}_{Li}^{\text{sim}}$ vertical loads acting on the vehicle wheels evaluated in a test performed with vehicle speed equal to V = 40 ms^{-1}, a car-body mass $M = 50$ t and different values of f_n, are listed in Table II. This case has been shown because it represents the worst case in terms of error. The good algorithm accuracy in estimating the vertical loads is mainly due to the capability of correctly describing the global shape of the input signals (both in space and in time) and not only the peaks, that are more affected by errors and noise. Table II shows the good accuracy

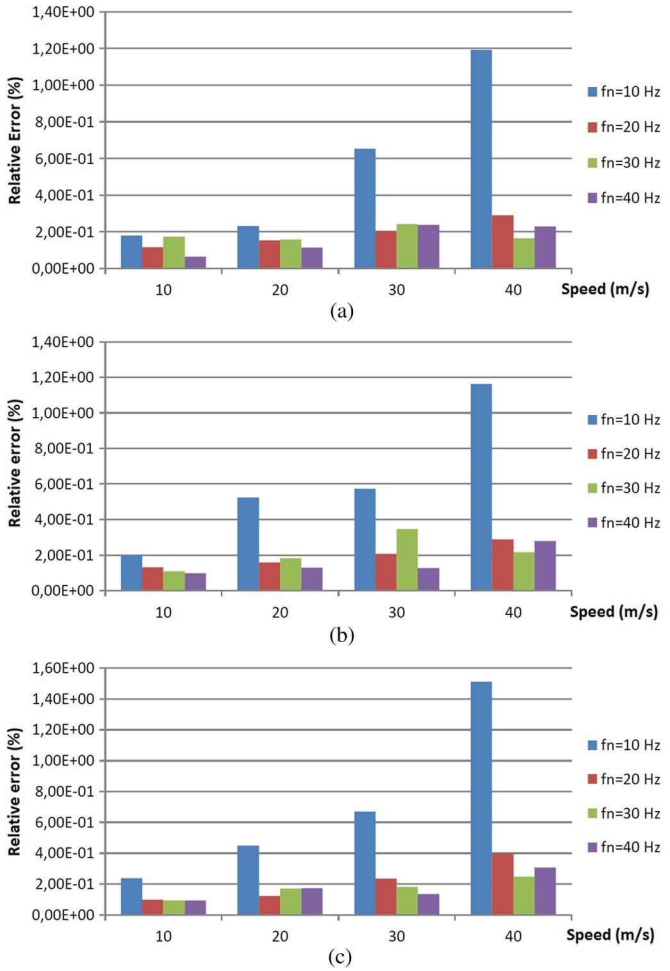

Fig. 10. Behavior of the relative error $e^{sim}_{max}(V, M, f_n)$ as a function of speed V, car-body mass M and cut-off frequency f_n. (a) M = 20 t. (b) M = 30 t. (c) M = 40 t.

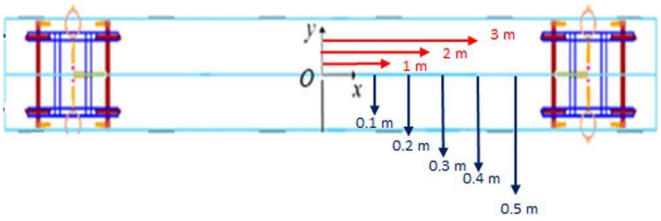

Fig. 11. Positions of car-body center of gravity $G_b = (X_b, Y_b)^T$ used to change $G_b = (X_G, Y_G)^T$.

of the *WIM* algorithm even for relatively low values of f_n. The maximum resulting error is equal to 1.9% and is related to a simulation performed considering the following values: V = 40 ms^{-1}, M = 50 t and f_n = 10 s^{-1}.

Fig. 10 shows a comparison among the maximum relative errors $e^{\text{sim}}_{\text{max}}(V, M, f_n)$ and their behavior as a function of speed V and cut-off frequency f_n; each graph is related to a different value of the vehicle car-body mass M.

Despite the good algorithm performance, these results show how the estimation of vertical loads becomes more difficult if the travel speed V increases and the cut-off frequency f_n decreases. In this case, the quasi-linearity hypothesis begins to be a critical condition and the adjacent wheel loads acting on the track can no longer be considered independent and superimposable.

TABLE III
LONGITUDINAL X_b AND LATERAL Y_b POSITIONS OF THE CENTER OF GRAVITY G_b OF THE CAR-BODY

X_b	Y_b
$X_b = 0.0$ m	$Y_b = 0.0$ m
$X_b = 1.0$ m	$Y_b = 0.1$ m
$X_b = 2.0$ m	$Y_b = 0.2$ m
$X_b = 3.0$ m	$Y_b = 0.3$ m
	$Y_b = 0.4$ m
	$Y_b = 0.5$ m

TABLE IV
RELATIVE ERRORS $e^{\text{sim}}_{\text{max}}$ ON THE ESTIMATED LOADS WITH DIFFERENT SPEEDS V AND LONGITUDINAL POSITIONS OF THE CAR-BODY CENTER OF GRAVITY X_b, PERFORMED WITH A CAR-BODY MASS M = 10 t AND A CUT-OFF FREQUENCY f_n = 20 s^{-1}

Position m	Par.	**Speed** 10 m s^{-1}	**Speed** 20 m s^{-1}	**Speed** 30 m s^{-1}	**Speed** 40 m s^{-1}
$X_b = 0$	0.10 %	0.16 %	0.26 %	0.26 %	
$X_b = +1$	0.19 %	0.16 %	0.20 %	0.42 %	
$X_b = +2$	0.19 %	0.24 %	0.25 %	0.33 %	
$X_b = +3$	0.17 %	0.29 %	0.19 %	0.37 %	

2) Estimation of the Longitudinal X_G and Lateral Y_G Positions of the Vehicle Center of Gravity G: The good accuracy exhibited by the new WIM approach in estimating the vertical loads acting on the wheels makes the novel algorithm suitable for the estimation of the longitudinal X_G and lateral Y_G positions of the vehicle center of gravity G, to avoid possible dangerous imbalances. The considered measurement layout is the one described in Par. V-A1.

The vehicle center of gravity G position has been varied in both longitudinal and lateral directions to simulate different unbalanced loads. The displacement values are established in such a range that satisfies the limits imposed by the real vehicle dimensions, with the aim of reproducing a real scenario. The actual longitudinal X_G, and the lateral Y_G positions of the vehicle center of gravity G have been varied by changing the position of the center of gravity of the car-body G_b (and hence X_b and Y_b), according to the values reported in Fig. 11 and Table III. The test campaign has been performed considering a car-body mass value M = 10 t, a cut-off frequency f_n = 20 s^{-1} and four different values of the vehicle velocity (V = 10, 20, 30, 40 ms^{-1}).

Table IV summarizes the maximum relative errors $e^{\text{sim}}_{\text{max}}$ on the estimated loads as a function of the vehicle speed V and the longitudinal displacement X_b of center of gravity G_b, performed with a car-body mass M = 10 t and a cut-off frequency f_n = 20 s^{-1}.

Fig. 12 shows the estimated loads $\hat{N}_R$, $\hat{N}_L$ with different values of the longitudinal displacement X_b performed at a vehicle speed V = 10 ms^{-1}: it can be seen that loads are perfectly symmetrical with respect to the longitudinal vehicle plane, being the center of gravity G placed along the longitudinal axis of the vehicle (the vehicle is not unbalanced along the lateral axis). The position of the car-body center of gravity G_b is translated longitudinally toward the head of the train, with a consequent increase of the loads acting on the wheels of the front bogie ($\hat{N}_{R_1}$, $\hat{N}_{L_1}$, $\hat{N}_{R_2}$, $\hat{N}_{L_2}$) and a decrease of the ones acting on the rear bogie (N_{R3}, N_{L3}, N_{R4}, N_{L4}). Regarding the algorithm robustness with respect to the measurement chain, Fig. 13 highlights the maximum errors for cut-off frequencies f_n from 10 s^{-1} to 40 s^{-1}: results are shown for two significant values of speed V, 20 ms^{-1} and 40 ms^{-1}, with the maximum longitudinal displacement of the center of gravity of the carbody X_b equal to +3 m and a vehicle mass M = 40 t.

Analogously, the next results are focused on the lateral displacement Y_G of the vehicle center of gravity for different values of speed V. Table V summarizes the behavior of the errors as a function of speed, performed with a car-body mass M = 40 t and a cut-off frequency f_n = 20 s^{-1}. A simulation campaign considering different unbalanced loads is reported: in particular, five steps of 0.1 m are considered along the lateral coordinate Y_b of the car-body center of gravity G_b and a slight increase of the errors with the speed can be observed.

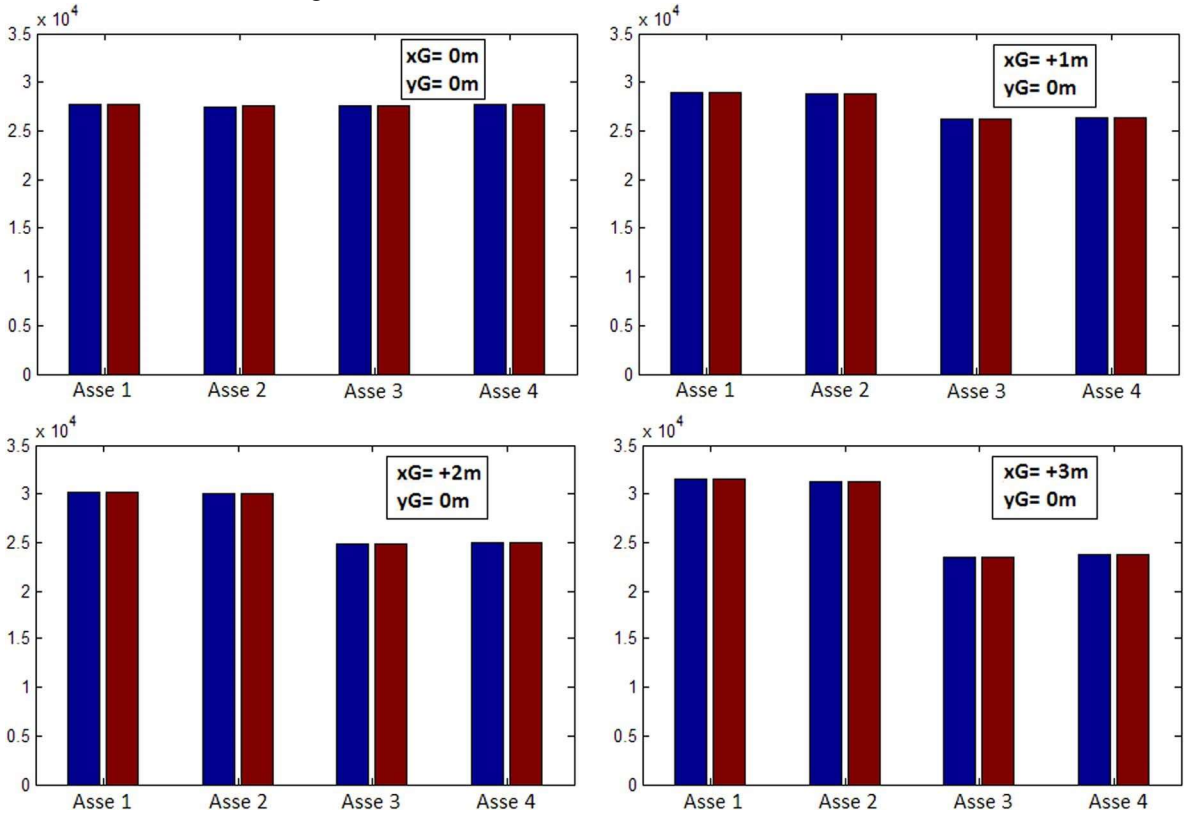

Fig. 12. Estimated loads $\hat{N}_R$, $\hat{N}_L$ with different values of longitudinal displacement X_b of the centre of gravity, performed at a vehicle speed V = 10 ms^{-1}. Blue bar: load on the left wheels—Red bar: load on the right wheels.

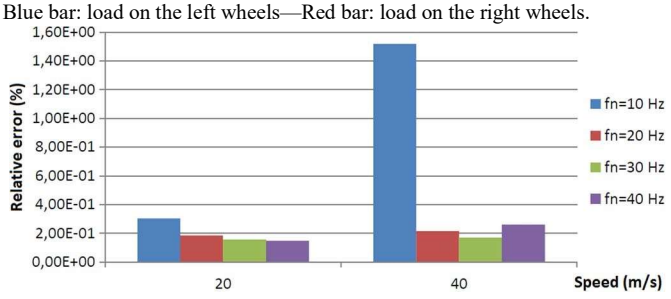

Fig. 13. Behavior of the maximum error as a function of speed V and cut-off frequency f_n (X_b = 3 m and vehicle mass M = 40 t).

TABLE V
RELATIVE ERRORS ON THE ESTIMATED LOADS WITH DIFFERENT SPEEDS V AND LATERAL POSITIONS OF THE CAR-BODY CENTER OF GRAVITY Y_b, PERFORMED WITH A CAR BODY MASS M = 10 t AND A CUT-OFF FREQUENCY f_n = 20 s^{-1}

Position m	**Speed** 10 m s^{-1}	**Speed** 20 m s^{-1}	**Speed** 30 m s^{-1}	**Speed** 40 m s^{-1}
$Y_b = 0$ (m)	0.13 %	0.14 %	0.20 %	0.27 %
$Y_b = +0.1$ (m)	0.15 %	0.15 %	0.251 %	0.278 %
$Y_b = +0.2$ (m)	0.19 %	0.24 %	0.28 %	0.213 %
$Y_b = +0.3$ (m)	0.17 %	0.29 %	0.19 %	0.22 %
$Y_b = +0.4$ (m)	0.17 %	0.29 %	0.19 %	0.22 %

As in the previous case, Fig. 14 shows the estimated $\hat{N}_R$, $\hat{N}_L$ loads with different values of the lateral displacement Y_b performedat a vehicle speed V = 10 ms^{-1}: in this scenario, the $\hat{N}_{R_1}$, $\hat{N}_{L_1}$, $\hat{N}_{R_2}$, $\hat{N}_{L_2}$

loads are quite asymmetrical with respect to the longitudinal plane, being the center of gravity G placed along the lateral axis of the vehicle (the vehicle is now unbalanced along the lateral axis). The position of the car-body center of gravity G_b is translated laterally toward the right side of the train, with a consequent increase of the loads acting on the right wheels of the vehicle ($\hat{N}_{R_1}$, $\hat{N}_{R_2}$, $\hat{N}_{R_3}$, $\hat{N}_{R_4}$) and a decrease of the ones acting on the left wheels (N_{L1}, N_{L2}, N_{L3}, N_{L4}).

Finally, in Fig. 15 the error trend as a function of speed V and cut-off frequency f_n has been reported, with a car-body mass M = 40 t and for a lateral displacement Y_b equal to 0.5 m. These results confirm the good performance of the proposed

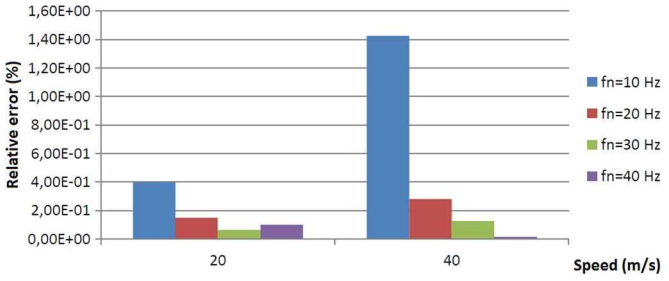

Fig. 15. Error trend as a function of speed V and cut-off frequency f_n (Y_b = 0.5 m, with a vehicle mass M = 40 t).

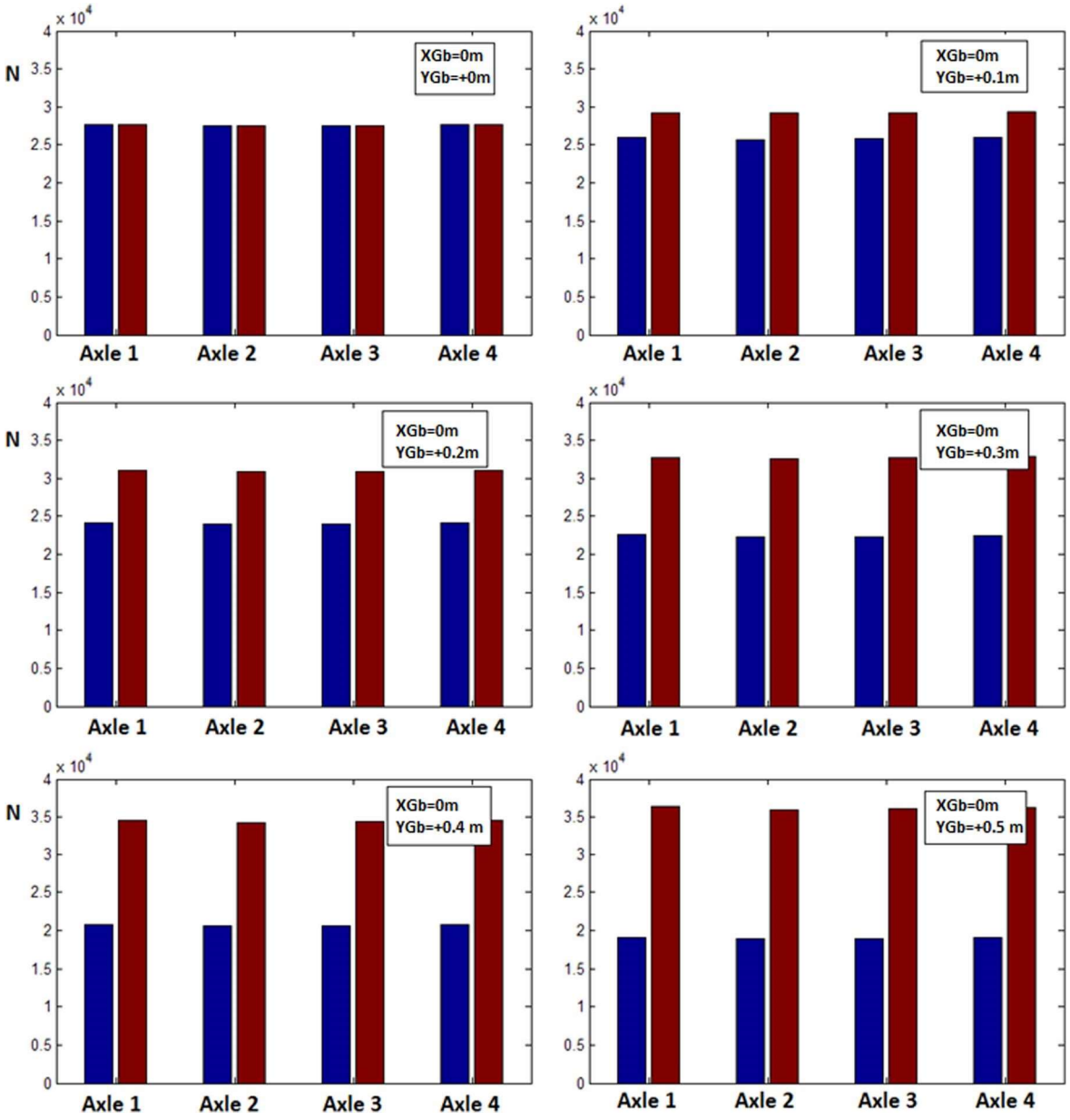

Fig. 14. Estimated loads $\hat{N}_R$, $\hat{N}_L$ with different values of lateral displacement Y_b of the car-body center of mass, performed with a vehicle speed V = 10 ms^{-1}. Blue bar: load on the left wheels—Red bar: load on the right wheels.

WIM algorithm in estimating unbalanced loads. Consequently, it can be effectively used to estimate the vehicle center of on the wheels.

gravity G, starting from the values of the vertical loads acting

VI. Conclusion and Further Developments

In this paper the authors present an new intelligent high speed WIM system aimed at automatically estimating the vertical wheel loads $\widehat{N}_{Ri}$, $\widehat{N}_{Li}$ and the longitudinal X_G and lateral Y_G position of the center of gravity G of railway vehicles to avoid possible dangerous imbalances.

The WIM algorithm is based on the measurement of the vertical forces acting on the sleepers F_z (the inputs of the algorithm) performed through force sensitive elements placed over the sleepers in the section corresponding to the rail baseplate/ pads. The new method can also manage different types of input signals (as the rail shear and bending, the longitudinal strain and stress on the rail, etc.). These physical quantities are then properly processed by means of suitable estimation procedures exploiting the quasi-linearity of the considered system and based on least squares optimization (LSO) techniques.

The performance of the WIM algorithm in terms of accuracy and robustness has been accurately studied. The algorithm has been tested for different values of velocity, car-body mass, cut frequency of the measurement chain and position of the vehicle center of mass. Results have shown the good performance of the new approach under any operating conditions.

Concerning the future developments, different estimation methods (like weighted least square optimization (WLSO) and nonlinear least square optimization (NLSO)) will be analyzed. Thanks to the algorithm capability of managing different types of physical inputs, further physical quantities as rail stresses σ and deformations ε will be considered as inputs of the procedure. From an experimental point of view, a simplified version of the proposed algorithm was partially and preliminary validated in [6]. However, more exhaustive experimental tests are scheduled for the future by Ansaldo STS and ECM Spa, the industrial partners of the project. Experimental data will mainly concern wagons travelling at high speeds and trains characterized by different geometries. Moreover further experimental campaigns will be performed on different railway tracks with different measurement layouts.

References

[1] M. Molodova, Z. Li, and R. Dollevoet, "Axle box acceleration: measurement and simulation for detection of short track defects," *Wear*, vol. 271, no. 1/2, pp. 349–356, May 2011.

[2] M. Molodova, Z. Li, A. Nunez, and R. Dollevoet, "Automatic detection of squats in railway infrastructure," *IEEE Trans. Intell. Transp. Syst.*, vol. 15, no. 5, pp. 1524–9050, Oct. 2014.

[3] S. Iwnicki, *Handbook of Railway Vehicle Dynamics*. New York, NY, USA: Taylor & Francis, 2006.

[4] J. Kisilowski and K. Knothe, *Advanced Railway Vehicle-System Dynamics*. Warsaw, Poland: Wydawnictwa Naukowo-Techniczne, 1991.

[5] K. Sekula and P. Kolakowski, "Identification of dynamic loads generated by trains in motion using piezoelectric sensors," in *Proc. ISMA*, Leuven, Belgium, 2010, pp. 1099–1118.

[6] E. Meli and L. Pugi, "Preliminary development, simulation and validation of a weigh in motion system for railway vehicles," *Meccanica*, vol. 48, no. 10, pp. 2541–2565, 2013.

[7] R. Mayer *et al.*, "Reducing the environmental impact of road and rail vehicles," *Environment. Impact Assessment Rev.*, vol. 32, no. 1, pp. 25–32, 2012.

[8] L. Poulikakos *et al.*, "In situ measurements of the environmental footprint of freight vehicles in switzerland," *Reducing Environ. Impact Road Rail Veh.*, vol. 13, no. 4, pp. 274–282, 2008.

[9] A. Rindi, L. Pugi, and E. Meli, "An innovative high speed weigh in motion system for railway vehicles," in *Proc. IEEE MESA Congr.*, Senigallia, Italy, Sep. 10–12, 2014, pp. 1–7.

[10] Official Site of Stock Equipment Company, 2012. [Online]. Available: http://www.stockequipment.com

[11] J. J. Kalker, *Three-Dimensional Elastic Bodies in Rolling Contact*. Dordrecht, Netherlands: Kluwer, 1990.

[12] A. Bracciali, R. Ciuffi, and F. Piccioli, "Progetto e validazione di un sensore estensimetrico multifunzionale per il binario ferroviario," in *Proc. 30th Congr. AIAS*, Alghero, Italy, 2001, pp. 901–912.

[13] C. del Prete and C. Rosso, "An easy instrument and a methodology for the monitoring and the diagnosis of a rail," *Mech. Syst. Signal Process.*, vol. 23, no. 3, pp. 940–956, Apr. 2009.

[14] Official Site of Kistler, 2012. [Online]. Available: http://www.kistler.com

[15] Official Site of Tagmaster, 2012. [Online]. Available: http://www.tagmaster.com

[16] P. Kolakowski and K. Sekula, "Piezo-based weigh-in-motion system for the railway transport," *Structural Control and Health Monitoring*, vol. 19, no. 2, pp. 199–215, Mar. 2010.

[17] C. Rowley, E. J. OBrien, A. Gonzalez, and A. Znidaric, "Experimental testing of a moving force identification bridge weigh-in-motion algorithm," *Exp. Mech.*, vol. 49, no. 5, pp. 743–746, Oct. 2009.

[18] E. J. OBrien, A. Znidaric, and T. Ojio, "Bridge weigh in motion latest developments and applications world wide," in *Proc. 5th Int. Conf. WeighIn-Motion*, Paris, France, May 19–22, 2008, pp. 25–38.

[19] C. Rowley, A. Gonzalez, E. J. OBrien, and A. Znidaric, "Comparison of conventional and regularized bridge weigh in motion algorithms," in *Proc. 5th Int. Conf. Weigh-In-Motion*, Paris, France, May 19–22, 2008, pp. 1–17.

[20] E. J. OBrien, A. Znidaric, and T. Dempsey, "Comparison of two independently developed bridge weigh-in-motion systems," *Int. J. Heavy Veh. Syst.*, vol. 6, no. 1, pp. 147–161, 1999.

[21] S. Falomi, M. Malvezzi, and E. Meli, "Multibody modeling of railway vehicles: Innovative algorithms for the detection of wheel-rail contact points," *Wear*, vol. 271, no. 1/2, pp. 453–461, 2011.

[22] E. Meli, S. Falomi, M. Malvezzi, and A. Rindi, "Determination of wheel—Rail contact points with semianalytic methods," *Multibody Syst. Dyn.*, vol. 20, no. 4, pp. 327–358, 2008.

[23] Official Site of Comsol Multiphysics, 2012. [Online]. Available: http://www.comsol.com

[24] Official Site of The MathWorks, 2012. [Online]. Available: http://www.mathworks.com

[25] C. Kelley, *Iterative Methods for Linear and Nonlinear Equations*. Philadelphia, PA, USA: SIAM, 1995.

[26] L. F. Shampine and M. W. Reichelt, "The matlab ode suite," *SIAM J. Scientific Computation*, vol. 18, pp. 1–22, 1997.

[27] J. Nocedal and S. Wright, *Numerical Optimization*. ser. Springer Series in Operation Research. Berlin, Germany: Springer-Verlag, 1999.

[28] T. Dahlberg, "Some railroad settlement models—A critical review," *J. Rail Rapid Transit*, vol. 215, no. 4, pp. 289–300, Apr. 2001.

[29] J. A. Zakeri, H. Xia, and J. J. Fan, "Dynamic responses of train-track system to single rail irregularity," *Latin Amer. J. Solids Structures*, vol. 6, no. 2, pp. 89–104, 2009.

[30] S. Iwnicki, *The Manchester Benchmarks for Rail Vehicle Simulators*. Lisse, The Netherland, Swets and Zeitlinger, 2008.

[31] M. Ignesti *et al.*, "Development of an innovative weigh in motion system for railway vehicles," in *Proc. ECCOMAS Thematic Conf. Multibody Dyn.*, Zagreb, Croatia, Jul. 1–4, 2013, pp. 763–768.

Benedetto Allotta received the Ph.D. degree from University of Pisa, Italy. He is currently a Professor of machine theory with the School of Engineering, University of Florence, and is the Cofounder and the Coordinator of the Laboratory of Mechatronics and Dynamic Modelling (MDM Lab). His current research interests include vehicle dynamics, mechatronics, robotics, sensor-based navigation of vehicles, hardware-in-the-loop (HIL) simulation, and automation in transport systems.

Pierluca D'Adamio is currently working toward the Ph.D. degree in machine theory with the School of Engineering, University of Florence. His current research interests include vehicle dynamics and autonomous vehicles.

Lorenzo Marini is currently working toward the Ph.D. degree in machine theory with the School of Engineering, University of Florence. His current research interests include vehicle dynamics and autonomous vehicles

Assistant Professor His current vehicle dynamics, control theory.

Enrico Meli is currently working toward the Ph.D. degree with the School of Engineering, University of Florence, where he is also an of machine theory and robotics. research interests include autonomous vehicles, and

Luca Pugi is currently working toward the Ph.D. degree with the School of Engineering, University of Florence, where he is also currently an Assistant Professor of machine theory and robotics His current research interests include vehicle dynamics, autonomous vehicles, and mechatronics.

Andrea Rindi received the Ph.D. degree from University of Florence, Italy. He is currently a Professor of machine theory with the School of Engineering, University of Florence. He is a Cofounder and the Coordinator of the Laboratory of Mechatronics and Dynamic Modelling (MDM Lab). His current research interests include vehicle dynamics, hardwarein-the-loop (HIL) simulation, and automation in transport systems.